Journal Pre-proofs

High-efficiency recognition and detection of sulindac in sewage using hydrophilic imprinted resorcinol-formaldehyde resin magnetic nano-spheres as SPE adsorbents combined with HPLC

Yue Wang, Wenchang Zhao, Xuemeng Tian, Huijia Song, Ruixia Gao, Xiaoshuang Tang, Xiaojing Zhang, Yi Hao, Yuhai Tang

PII: S1385-8947(19)33131-6
DOI: https://doi.org/10.1016/j.cej.2019.123716
Reference: CEJ 123716

To appear in: *Chemical Engineering Journal*

Received Date: 27 August 2019
Revised Date: 3 December 2019
Accepted Date: 4 December 2019

Please cite this article as: Y. Wang, W. Zhao, X. Tian, H. Song, R. Gao, X. Tang, X. Zhang, Y. Hao, Y. Tang, High-efficiency recognition and detection of sulindac in sewage using hydrophilic imprinted resorcinol-formaldehyde resin magnetic nano-spheres as SPE adsorbents combined with HPLC, *Chemical Engineering Journal* (2019), doi: https://doi.org/10.1016/j.cej.2019.123716

High-efficiency recognition and detection of sulindac in sewage using hydrophilic imprinted resorcinol-formaldehyde resin magnetic nano-spheres as SPE adsorbents combined with HPLC

Yue Wang[a,†], Wenchang Zhao[a,†], Xuemeng Tian[a], Huijia Song[a], Ruixia Gao[a,*], Xiaoshuang Tang[c], Xiaojing Zhang[a], Yi Hao[b,*], Yuhai Tang[a]

[a] *School of Science, Xi'an Jiaotong University, Xi'an, Shaanxi 710049, China*

[b] *School of Pharmacy, Health Science Center, Xi'an Jiaotong University, Xi'an, Shaanxi 710061, China*

[c] *Department of Urology, The Second Affiliated Hospital of Xi'an Jiaotong University, Xi'an, Shaanxi 710061, China*

† Yue Wang and Wenchang Zhao contributed equally to this work and are co-first authors.

* Corresponding authors:

E-mail: ruixiagao@xjtu.edu.cn (R. Gao); haoyi8904@xjtu.edu.cn (Y. Hao).

Tel: +86 29 82655399; fax: +86 29 82655399.

Abstract

Hydrophilic molecularly imprinted polymer for effective removal of pollutants from environmental water has attracted much attention due to their high selectivity and matrix compatibility. Herein, resorcinol and formaldehyde have been first proposed as the hydrophilic monomers to form water-compatible molecularly imprinted resin magnetic nanomaterials (Fe_3O_4-RF-MIPs) by adopting a two-step template immobilization strategy of surface molecular imprinting technique. In the synthesis process, carboxyl-modified Fe_3O_4 nanoparticles and sulindac were adopted as carrier and template molecule, respectively. The physical and chemical properties, preparation process, and adsorption conditions of Fe_3O_4-RF-MIPs were investigated in detail. Fe_3O_4-RF-MIPs exhibit uniform morphology, high crystallinity, outstanding magnetic property, fast binding kinetics, high adsorption capacity, satisfactory selectivity, and excellent reusability. Meanwhile, combining with HPLC, Fe_3O_4-RF-MIPs as solid phase extraction adsorbents have been successfully applied to specifically enrich and detect sulindac in sewage water. Accordingly, Fe_3O_4-RF-MIPs with ordered and evenly distributed imprinted sites and excellent dispersibility in water would be potential in the field of water environmental pollution control.

Keywords: Hydrophilic molecularly imprinted polymers; Resorcinol-formaldehyde resin; Sulindac; Magnetic separation

1. Introduction

Pharmaceutical and Personal Care Products (PPCPs), as emerging pollutants, have received increasing attention [1]. PPCPs include various types of antibiotics, synthetic musk, antihypertensive drugs, hair dyes, and nonsteroidal anti-inflammatory drugs [2]. Sulindac (SLA), one of the nonsteroidal anti-inflammatory drugs, was approved for use by the FDA in 1978 [3]. It has been used to treat various inflammations for more than 30 years with annual sales of several hundred tons. A lot of expired or excreted SLA in feces and urine are put into environmental water, which unfortunately return to the human body through the ecosystem. If excessive SLA molecules are accumulated in the human body, it is easy to cause abdominal pain, dizziness, and nausea, even causing seriously causing heart failure, depression, organ failure, and Steven-Johnson syndrome [4]. Thus, it is of prime importance to separate and detect SLA in the environmental water.

At present, the detection methods for SLA include UV spectrophotometer [5], capillary zone electrophoresis [6], HPLC [7], electrochemical [8], and Ultra-performance liquid chromatography [9]. The above methods often need sample pretreatment, and the common sample pretreatment methods include solid phase extraction (SPE), accelerated solvent extraction, supercritical fluid extraction, and liquid-liquid extraction [10-13]. Among them, SPE has gained widespread concern due to the advantages of rapidity, simplicity, less use of organic solvents, and good reproducibility. However, the traditional SPE adsorbents still need complex centrifugation procedures and lack selectivity. Therefore, new SPE adsorbents with

specific recognition ability for enrich of trace SLA are urgently required. Molecularly imprinted polymers (MIPs) have tailor-made binding sites that match well with the shapes, sizes, and functional groups of predetermined template molecules [14]. We reason that MIPs might be ideal SPE adsorbents for sample pretreatment.

During the past decades, surface molecular imprinting technique is regarded as an effective method to synthesize MIPs by virtue of having plenty of recognition sites on the surface of carriers. Compared with MIPs synthesized by bulk polymerization, more uniform and effective binding sites exist on the surface of solid carriers, which makes template molecules easier to be eluted, speeds up the mass transfer rate, and reduces template leakage [15]. Due to these superiorities, MIPs prepared by surface molecular imprinting technique as SPE adsorbents have been widely used. Numerous nano-structural materials (quantum dots [16], carbon nanotubes [17], SiO_2 [18] or magnetic nanoparticles [19]) are used as solid carriers for surface imprinting of PPCPs because of their special characteristics of high surface-to-volume ratio and physical/chemical properties related to particle size. Thereinto, magnetic Fe_3O_4 nanoparticles have received particular attention owing to their good biocompatibility, low toxicity, and superparamagnetism [20].

To date, most MIPs are synthesized by co-polymerization of hydrophobic functional monomers and template molecules with a crosslinking agent in organic or rich-organic solvents, and exhibit good adsorption performance in the corresponding organic solvents [21-23]. However, when these MIPs are applied in aqueous matrices such as food, medical, and environmental fields, they mostly fail to show high

adsorption capacity and outstanding selectivity, which attributes to the incompatibility of MIPs with aqueous solutions and interference caused by water molecules through impairing the hydrogen bond forces between template molecules and imprinted sites [24,25]. In addition, a great quantity of organic solvents required for the preparation of MIPs is quite harmful to environment and human health. These two shortcomings greatly limit the practical application of MIPs. Therefore, the development of hydrophilic MIPs is necessary. In order to increase the hydrophilicity of MIPs, adopting hydrophilic monomers to prepare MIPs is an effective solution. Zaidi et al. [26] adopted dopamine as the functional monomer to prepare the hydrophilic MIPs for efficiently extracting 6-thioguanine in samples of urine. Xu et al. [27] described a kind of hydrophilic MIPs using 2-acrylamido-2-methylpropane sulfonic acid as the functional monomer for selective adsorption of trace acrylamide in food samples. Zhu et al. [28] utilized 1-allyl-3-vinylimidazole chloride and 2-hydroxyethyl methacrylate as the functional monomers to synthesize the hydrophilic MIPs for selective adsorption of ciprofloxacin in environmental water. Compared with the previous hydrophobic MIPs for the above corresponding three targets [29-31], the adsorption capacity and the imprinting factor of hydrophilic MIPs are increased by 2.3 to 3.4 times and 1.2 to 6.2 times, respectively. Up to now, only a few hydrophilic functional monomers have been developed. Thus, it is still of great challenge to explore new hydrophilic functional monomers for preparing MIPs with satisfactory molecular recognition ability in water-based matrices.

Hydrophilic resins (e.g. resorcinol-formaldehyde resin, epoxy resin, acrylic resin,

chitosan-glyoxal resin, styrene-maleic acid-functionalized resin, etc.) show excellent potential for preparing water-compatible MIPs. Yuan et al. [32] prepared hydrophilic protein-imprinted resin by using resorcinol and melamine as functional monomers for selective adsorption of bovine serum albumin in the aqueous matrix. Monier et al. [33] synthesized imprinted styrene-maleic acid-functionalized resin for enantioselective extraction of R-amphetamine. They also fabricated chitosan/glutaraldehyde resin for enantioselective separation of L-glutamic acid [34]. Cao et al. [35] developed hydrophilic melamine-urea-formaldehyde monolithic resin for specific recognition of plant growth regulators in water. These synthesized hydrophilic MIPs have specific recognition ability and high enrichment efficiency in water. But, when directly used as SPE adsorbents, they need to be ground, screened, and centrifuged, which is time-consuming and complicated. In addition, the preparation processes using these functional monomers [36-38] need to be added additional reagents as crosslinking agents and heated to synthesize hydrophilic resins. To address these issues, we select resorcinol and formaldehyde as the hydrophilic functional monomers combining with magnetic Fe_3O_4 nanoparticles to prepare hydrophilic molecularly imprinted resorcinol-formaldehyde resin magnetic nano-spheres with high adsorption property and rapid separation efficiency. Resorcinol-formaldehyde resin has the advantages of abundant hydrophilic groups, good compatibility with the matrix, and mild preparation conditions. So far, to the best of our knowledge, there is no MIPs as SPE adsorbents for specific isolation of SLA, let alone for water-compatible magnetic MIPs for SLA.

Herein, we first adopt resorcinol and formaldehyde as the hydrophilic monomers, SLA as template molecule, and carboxyl modified Fe_3O_4 as carrier to form water-compatible molecularly imprinted resin magnetic nanomaterials by adopting a two-step template immobilization strategy. The two-step template immobilization strategy means that the template molecules are first immobilized with the functional groups on the surface of the carriers through covalent or non-covalent interaction, and then the template molecules are secondly immobilized using imprinted layer [39]. MIPs prepared by a two-step template immobilization strategy have more ordered imprinted sites and evenly distributed imprinted sites attached on the surface of carriers [40] compared to MIPs prepared by the one pot method. As we expected, the adsorption ability and selectivity of MIPs are improved by adopting a two-step template immobilization strategy, and the dispersibility of as-prepared MIPs in water is greatly improved because the resorcinol-formaldehyde resin imprinted layer contains a lot of hydrophilic groups. The preparation conditions were optimized in detail. Meanwhile, the characterization and binding capacities of synthesized MIPs were investigated. Moreover, a method for selective recognition and determination of SLA in environmental water samples was established by a combination of the obtained MIPs as SPE sorbents and HPLC.

2. Experimental

2.1. Materials and reagents

Ferric chloride hexahydrate ($FeCl_3 \cdot 6H_2O$), anhydrous sodium acetate (NaOAC), sodium polyacrylate (PPAS), ethanol, acetonitrile, acetic acid, ethylene glycol (EG),

diethylene glycol (DEG), and ammonium hydroxide ($NH_3 \cdot H_2O$, 25%) were purchased from Xi'an Chemicals Ltd. Resorcinol (RSC), formaldehyde (FMD), sulindac (SLA), indole (ID), indomethacin (NA), 3-indoleacetic acid (IAA), benzidamine hydrochloride (BZD), estradiol (E2), and estrone (E1) were obtained from Shanghai Aladdin Ltd. The highly purified water (18.25 MΩ/cm) was prepared with a WaterPro water system (Axlwater Corporation, TY10AXLC1805-2, China) and used throughout the experiments. All reagents are of at least analytical grade and used without further treatment.

2.2. Preparation of Fe_3O_4-COOH

According to previous reports [40], the carboxyl-modified Fe_3O_4 magnetic nanomaterials (designed as Fe_3O_4-COOH) were obtained by a one-step solvothermal method. Firstly, the $FeCl_3 \cdot 6H_2O$ (0.51 g), NaOAC (2.03 g), and PPAS (0.05 g) were dispersed into the mixture of EG (7 mL) and DEG (15 mL). Then, the solution was poured into high pressure reactors, sealed to heat at 200 °C. After reaction for 12 h, the autoclave was cooled to room temperature. Subsequently, the products were repeatedly washed with highly purified water and dried under vacuum at 40 °C to constant weight. Finally, Fe_3O_4-COOH were obtained by grinding.

2.3. Preparation of Fe_3O_4-RF-MIPs

The magnetic imprinted nanomaterials with resorcinol-formaldehyde resin and Fe_3O_4-COOH as the imprinted layer and carrier, respectively (designed as Fe_3O_4-RF-MIPs) were synthesized by a two-step template immobilization strategy. Firstly, 0.25 g of Fe_3O_4-COOH were dispersed into 20.0 mL of highly purified water

in a 100 mL of three-necked bottle and the mixture was sonicated for 10 min. Then, 0.30 g of SLA and 2.0 mL of $NH_3 \cdot H_2O$ (25%) were added and stirred for 30 min. Afterward, 0.10 g of RSC and 0.05 mL of FMD were added to the above mixed solution, mechanically stirring for 6 h. Subsequently, the prepared nanomaterials were cured for 10 hours and repeatedly washed with highly purified water. Finally, to remove the template molecules SLA, the method of adopting ethanol-acetic acid (95:5, v/v) as eluent and assisting shaking was used. 20.0 mL of eluent was replaced at intervals of two hours until no adsorption was detected at about 286 nm by HPLC. Through an external magnetic field, the obtained Fe_3O_4-RF-MIPs were separated from the eluent and washed with highly purified water for six times, then dried under vacuum at 40 °C. For contrast, non-imprinted magnetic nanomaterials (designed as Fe_3O_4-RF-NIPs) were synthesized by the same procedures without the presence of the template molecules SLA. In order to embody the advantages of two-step template immobilization strategy, Fe_3O_4-RF-MIPs and Fe_3O_4-RF-NIPs were synthesized by the one pot method with the same dosage and under the same conditions (Supporting Information).

2.4. Characterization

Morphological characters of the products were observed by field transmission electron microscope (TEM, jem-2100, Japan). Fourier transform infrared (FT-IR) spectra in the region of 400-4000 cm^{-1} were obtained by a Nicolet AVATAR 330 FT-IR spectrophotometer. The magnetic properties were analyzed at room temperature *via* a vibrating sample magnetometer (VSM, MPMS-squid VSM-094).

The identification of the crystalline phase was recorded with a Rigaku D/max/2500v/pc X-ray diffractometer (Rigaku Co., Japan) with Cu Kα radiation. The HPLC analyses were performed on a Hitachi HPLC system equipped with L-2130 pump, L-2400 detector, L-2300 column oven, and WondaSil C18 column (5 μm, 4.6 mm × 150 mm). The column temperature was 40 °C. The optimized mobile phase was acetonitrile (0.05%)-acetic acid solution (70:30, v/v) delivered at a flow rate of 1.0 mL min^{-1}, the injection volume was 10 μL, and the column effluent was monitored at 286 nm.

2.5. Adsorption experiments and selectivity evaluation

In the kinetic and isothermal adsorption experiments, the adsorption procedure was operated by adding 10.0 mg of Fe_3O_4-RF-MIPs or Fe_3O_4-RF-NIPs into 10.0 mL of SLA solution. The kinetic adsorption experiments were implemented by adjusting absorption time from 0 to 30 min at regular intervals, while the concentration of SLA was kept at 300 μg mL^{-1}. Then the nanoparticles were separated by an external magnetic field and the residual SLA in the supernatant was determined by HPLC. The adsorption amounts (Q, mg g^{-1}) of Fe_3O_4-RF-MIPs or Fe_3O_4-RF-NIPs to SLA were calculated on the basis of Eq. (1). The kinetic data were used to fit the Pseudo-second-order kinetic model based on Eq. (2).

$$Q = (C_0 - C_e)\, V / W \quad (1)$$

$$t / Q_t = 1 / k_2 Q_e^2 + t / Q_e = 1 / V_0 + t / Q_e \quad (2)$$

Where C_0 and C_e (μg mL^{-1}) respectively represent the initial and equilibrium concentration of SLA. V (mL) represents the volume of the SLA solution and W (g)

is the mass of the nanoparticles. k_2 (g $mg^{-1}min^{-1}$) is the equilibrium rate constant of pseudo-second-order equation. V_0 (mg $g^{-1}min^{-1}$) is the initial adsorption rate. Q_e is the equilibrated adsorption capacity and Q_t is the adsorption capacity at the time of t (min) [41,42].

The isothermal adsorption experiments were carried out by using SLA solutions with different initial concentrations in the range of 10-400 μg mL^{-1} under the same incubation time of 10 min. The process of separation and detection is the same as kinetic adsorption. The Freundlich isothermal model was used to analyze the adsorption process. It is defined as Eq. (3).

$$\log Q = m\log C_e + \log K_F \quad (3)$$

Where K_F (mg g^{-1}) is the Freundlich constant. m is the Freundlich exponent, expressing the system's heterogeneity [43].

The selectivity of Fe_3O_4-RF-MIPs was evaluated by selecting six compounds (ID, NA, IAA, BZD, E2, and E1) as the competitors. Accordingly, 10 mg of Fe_3O_4-RF-MIPs or Fe_3O_4-RF-NIPs were added into 10.0 mL of solution containing adsorbates at an initial concentration of 300 μg mL^{-1} and shaken for 10 min. The remaining steps were as the same to kinetic adsorption experiments.

The specific recognition ability of Fe_3O_4-RF-MIPs was evaluated by imprinting factor (*IF*) and selectivity coefficient (*SC*), which were defined as Eqs. (4) and (5).

$$IF = Q_{MIP} / Q_{NIP} \quad (4)$$

$$SC = IF_t / IF_c \quad (5)$$

Where Q_{MIP} and Q_{NIP} (mg g^{-1}) are the adsorption capacities to SLA or competitors

on Fe_3O_4-RF-MIPs and Fe_3O_4-RF-NIPs. IF_t and IF_c represent the imprinting factors for SLA and its competitors [41,44].

2.6. Reproducibility and reusability of Fe_3O_4-RF-MIPs

To evaluate the reproducibility of Fe_3O_4-RF-MIPs, 10.0 mg of six different batches of nanomaterials prepared on different days were added to 10.0 mL of SLA solution (300 μg mL^{-1}) and shaken for 10 min. Subsequently, Fe_3O_4-RF-MIPs were isolated by an additional magnet. The concentration of SLA in the supernatant was detected by HPLC.

Eight adsorption-desorption experiments of Fe_3O_4-RF-MIPs were performed adopting the same batch of nanomaterials to evaluate the reusability. 10.0 mg of Fe_3O_4-RF-MIPs were added to 10.0 mL of SLA solution (300 μg mL^{-1}) and shaken for 10 min. Subsequently, Fe_3O_4-RF-MIPs were isolated by an additional magnet. The concentration of SLA in the supernatant was detected by HPLC. The adsorbed nanomaterials were eluted with ethanol-HAc (95:5, v/v) for 6 h to ensure complete removal of the residual SLA in the polymers. At last, Fe_3O_4-RF-MIPs were dried in the vacuum at 40 °C for 2 h and then reused in the succeeding adsorption-desorption cycles.

2.7. Real sample analysis

To evaluate the adsorption ability of Fe_3O_4-RF-MIPs in practical application, the discharged sewage samples were collected from the Ruixin Pharmaceutical Plant and the Second Affiliated Hospital of Xi'an Jiaotong University (Xi'an, China). The discharged sewage samples were filtered by 0.22 μm membranes to remove the

suspended materials. Specifically, 10.0 mg of Fe_3O_4-RF-MIPs were dispersed into 10.0 mL of SLA spiked sewage samples at three different levels (0.01, 0.05, and 0.5 μg mL^{-1}). The mixed solution was shaken for 10 min. Subsequently, the adsorbed nanomaterials were washed by ethanol-HAc (95:5, v/v) for 6 h and the eluent was collected and evaporated to dry under a stream of nitrogen. Then the residues of the eluent were dissolved in 0.5 mL of acetonitrile. Finally, the standard, spiked, and eluted samples were used for the HPLC analysis.

3. Results and discussion

3.1. Synthesis of Fe_3O_4-RF-MIPs

The synthetic process of Fe_3O_4-RF-MIPs was exhibited in Fig. 1. First, Fe_3O_4-COOH were obtained by a one-step solvothermal method [40]. Then the template molecules SLA were immobilized at the surface of Fe_3O_4-COOH through multiple hydrogen bonding interactions between carboxyl groups of Fe_3O_4-COOH and the hydroxyl group, thionyl group, and fluorine atom of SLA to form Fe_3O_4-COOH-SLA complexes. Afterward, the resorcinol-formaldehyde resin imprinted layer embedding SLA was synthesized and covered on the Fe_3O_4-COOH by adding RSC and FMD. Because a lot of hydroxyl and phenyl groups existed in resorcinol-formaldehyde resin, SLA were further immobilized on Fe_3O_4-COOH through multiple hydrogen bonds and π-π interactions. In order to form more ordered and evenly distributed imprinted sites, resorcinol-formaldehyde resin as a new kind of hydrophilic imprinted layer was adopted to re-immobilize the template molecules. Finally, the SLA molecules were eluted with ethanol-HAc (95:5, v/v) and the

Fe_3O_4-RF-MIPs with specific imprinted sites to SLA were obtained. The specific adsorption capacity of Fe_3O_4-RF-MIPs is mainly attributed to the shape and size of the imprinted sites and specific noncovalent interactions (Supporting Information).

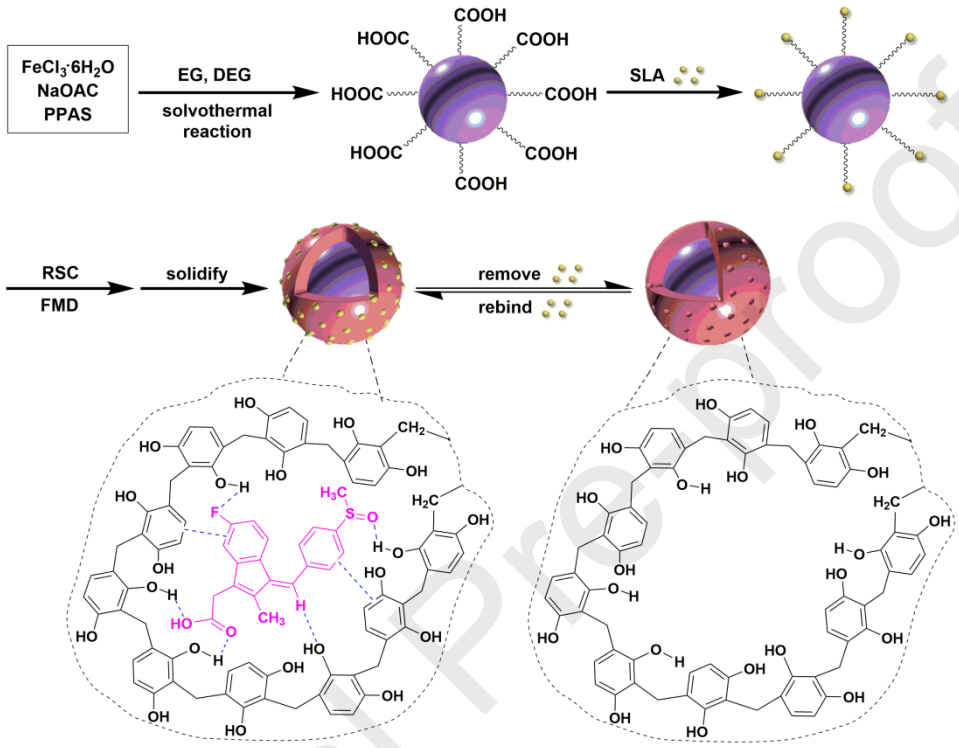

Fig. 1. The synthesis process of Fe_3O_4-RF-MIPs.

In order to get good recognition ability and the best thickness of imprinted layer, the ratio and amounts of RSC and FMD were optimized. As shown in Fig. 2A, the *Q* and *IF* display a growing trend with the ratio of RSC and FMD increasing. When the ratio of RSC and FMD is increased to 1:2, the *Q* (36.0 mg g^{-1}) and *IF* (4.36) reach to the maximum, which can be attributed to the fact that as the ratio of RSC and FMD increases, the polymers of RSC and FMD change from monohydric phenol to dihydric phenol to form linear resorcinol-formaldehyde resin. The linear resorcinol-formaldehyde resin with more exposed hydroxyl groups can interact with

SLA through multiple hydrogen bonds and π-π interactions. However, as the ratio of RSC and FMD is higher than 1:2, the resorcinol-formaldehyde resin generates a lot of ether bonds and plenty of hydroxyl sites are covered, reducing the binding sites of the resin to the SLA template molecules [45].

We also investigate the amount of RSC while maintaining the ratio of RSC and FMD at 1:2 (Fig. 2B). When RSC is less than 0.10 g, the adsorption capacity is smaller. This result can be interpreted as the fact that the limited RSC and FMD are not enough to provide recognition sites for all template molecules. When the amount of RSC is 0.10 g, the maximum amount of adsorption is obtained. This reason can be explained by the possibility that RSC and FMD are completely reacted, and form an appropriate imprinted layer with sufficient recognition sites to bind to the template molecules SLA. However, when the amount of RSC is more than 0.10 g, the adsorption capacity decreases. Because excessive RSC and FMD are self-polymerized and formed many resorcinol-formaldehyde resins floating in the reaction solution, so that some resins are not coated on the surface of nanoparticles (Fig. S1). In addition, this also causes reagent waste and post-processing difficulties. Therefore, the ratio of 1:2 of RSC and FMD and 0.10 g of RSC are adopted in our following experiments.

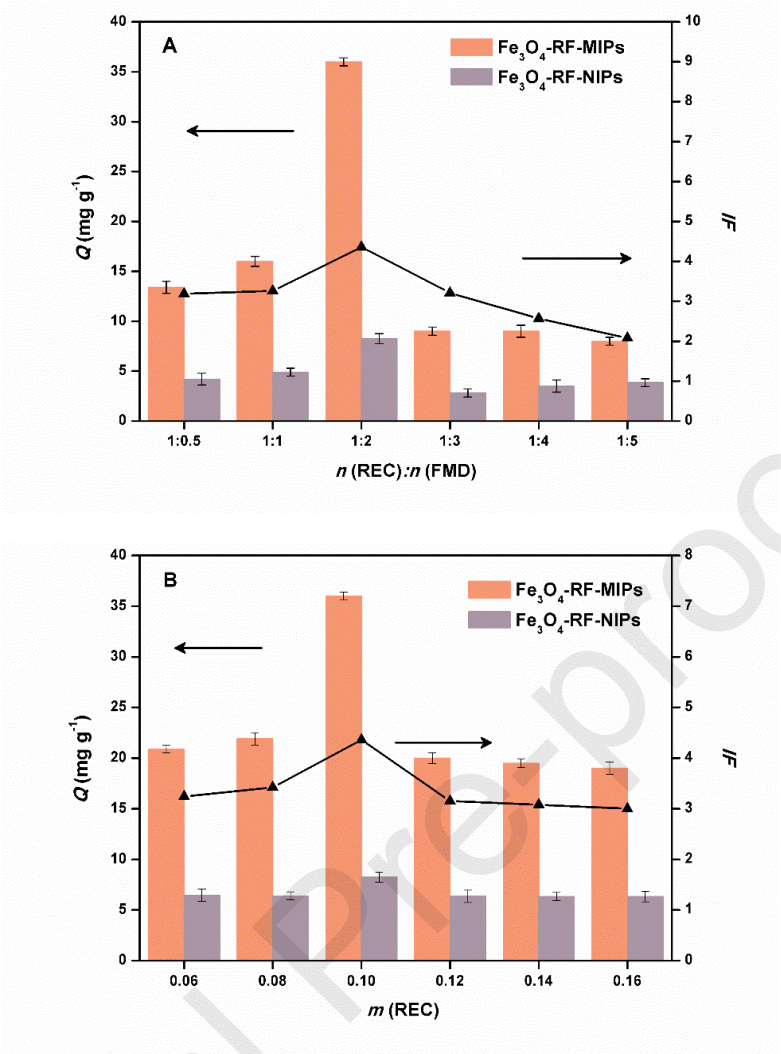

Fig. 2. Effect of the ratio of RSC and FMD (A) and the amount of RSC (B) on the imprinting performance of Fe_3O_4-RF-MIPs and Fe_3O_4-RF-NIPs.

3.2. Characterization of obtained nanomaterials

The TEM images of Fe_3O_4-COOH and Fe_3O_4-RF-MIPs are displayed in Fig. 3. Fe_3O_4-COOH in Fig. 3A have a spherical shape with a diameter of ~100 nm and uniform particle size distribution. Fig. 3B exhibits obviously ~30 nm thick layer on the Fe_3O_4-COOH, demonstrating the successful imprinted process. Meanwhile, the high resolution of TEM images with visible details have been presented in Fig. S2.

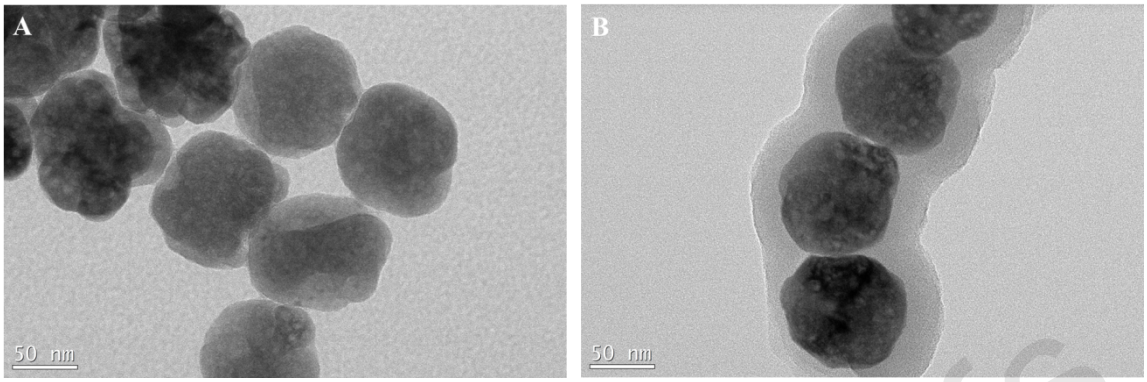

Fig. 3. TEM images of Fe_3O_4-COOH (A) and Fe_3O_4-RF-MIPs (B).

Fig. 4 shows the measured FT-IR spectra of Fe_3O_4-COOH and Fe_3O_4-RF-MIPs. The characteristic peaks of Fe-O are all observed at 578 cm^{-1} for Fe_3O_4-COOH and Fe_3O_4-RF-MIPs, indicating that magnetic nanoparticles are successfully synthesized. The absorption peaks at 3420 cm^{-1} and 1623 cm^{-1} are arisen from the stretching vibrations of O-H and C=O respectively [40]. It is manifested that Fe_3O_4-COOH are prepared by a one-pot solvothermal method. The peculiar four peaks at 1491, 1300, 961, and 725 cm^{-1} are assigned to the stretching vibration of $-CH_2-$, stretching vibration of O-H, bending vibration of C-H, and benzene ring framework bending vibration of C=C, suggesting that resorcinol-formaldehyde resin imprinted layer is successfully formed and the obtained nanoparticles have a large number of hydrophilic groups, which are beneficial to the dispersibility of Fe_3O_4-RF-MIPs in water. All these typical peaks reveal the successful formation of Fe_3O_4-RF-MIPs. The XRD patterns of Fe_3O_4-COOH (Fig. S3a) and Fe_3O_4-RF-MIPs (Fig. S3b) indicate that they both have a crystal form of Fe_3O_4 [46], but the peaks of Fe_3O_4-RF-MIPs are weaker than those of Fe_3O_4-COOH, which also proves that the surface of Fe_3O_4-RF-MIPs are covered with the imprinted layer.

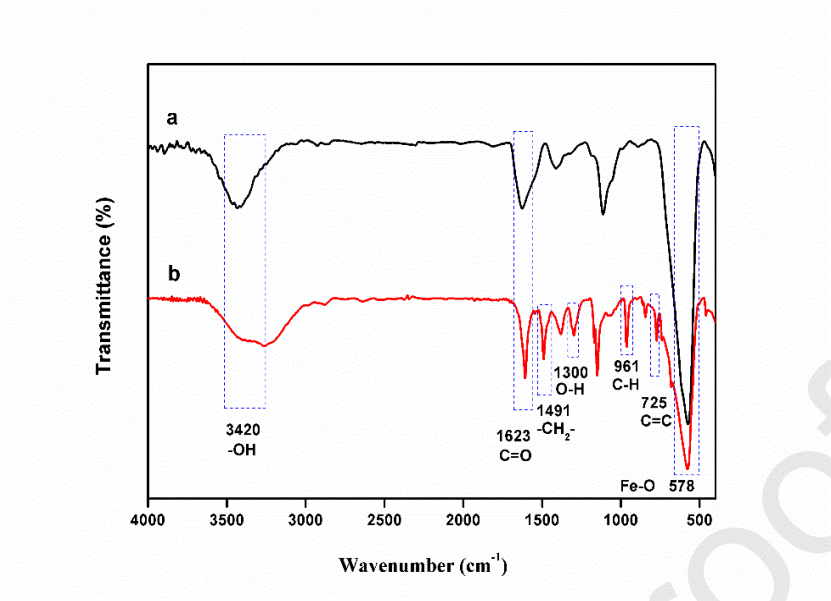

Fig. 4. FT-IR spectra of Fe_3O_4-COOH (a) and Fe_3O_4-RF-MIPs (b).

Fig. 5 depicts the magnetic properties of the Fe_3O_4-COOH and Fe_3O_4-RF-MIPs. The S-like curves demonstrate that magnetization saturation values of Fe_3O_4-COOH and Fe_3O_4-RF-MIPs are 79 and 56 emu g^{-1}. The reduction of magnetization saturation value of about 30% also indactes that the resorcinol-formaldehyde resin imprinted layer is successfully formed on the surface of Fe_3O_4-COOH. Fe_3O_4-RF-MIPs still possess enough magnetism to meet the demand of rapid magnetic separation. Meanwhile, the separation and redispersion processes of Fe_3O_4-RF-MIPs are displayed in Fig. S4. The synthesized Fe_3O_4-RF-MIPs can be readily dispersed in solution and when an additional magnet is placed next to them, the magnetic nanomaterials are strongly attracted to the place near the magnet. After the removal of the magnet, the redispersion of Fe_3O_4-RF-MIPs is achieved within three seconds.

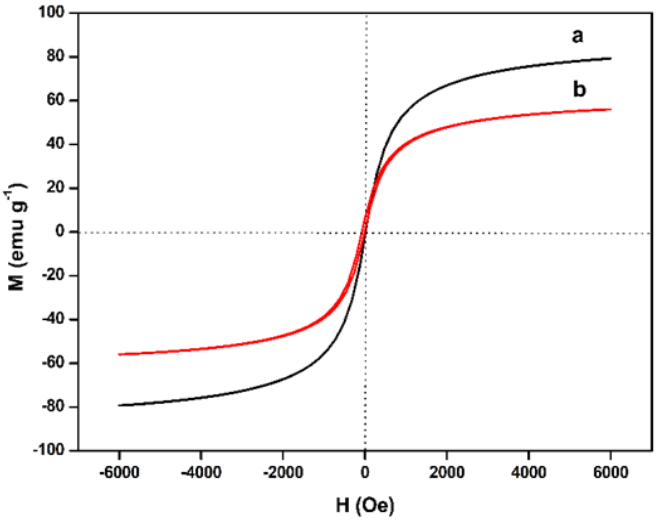

Fig. 5. Magnetization curves of Fe_3O_4-COOH (a) and Fe_3O_4-RF-MIPs (b).

3.3. Adsorption kinetics

The adsorption kinetics of SLA onto Fe_3O_4-RF-MIPs and Fe_3O_4-RF-NIPs are shown in Fig. 6A. The adsorption amount of Fe_3O_4-RF-MIPs increases rapidly in the first 2 min which reveals that there are a lot of available recognition sites. Then, the adsorption capacity reaches the equilibrium after 10 min, because the imprinted sites are gradually filled by the SLA template molecules. Fig. 6B exhibits that the experimental data for Fe_3O_4-RF-MIPs and Fe_3O_4-RF-NIPs are consistent with the Pseudo-second-order model (R^2 > 0.99). Table S1 exhibits the relevant kinetic parameters and equations, and the values of Q_e and k_2 are 37.04 g mg g^{-1}, 0.0384 g mg^{-1} min^{-1}, and 8.26 mg g^{-1}, 0.5428 g mg^{-1} min^{-1} for Fe_3O_4-RF-MIPs and Fe_3O_4-RF-NIPs, respectively. The V_0 of Fe_3O_4-RF-MIPs (52.63 mg g^{-1} min^{-1}) is much higher than that of Fe_3O_4-RF-NIPs (37.04 mg g^{-1} min^{-1}), suggesting that the adsorption of SLA by Fe_3O_4-RF-MIPs is a fast process because of the high density of recognition cavities at the surface of the Fe_3O_4-RF-MIPs. In addition, the chemical course can be considered as the rate-limiting step in the whole adsorption process

375 [42].

376 *3.4. Adsorption isotherms*

377 The isothermal adsorption of Fe_3O_4-RF-MIPs and Fe_3O_4-RF-NIPs toward SLA are
378 presented in Fig. 6C. The adsorption capacities of two absorbents gradually increase
379 with the concentration of SLA increasing, and attain saturation when the
380 concentration of SLA is 300 μg mL^{-1}. The adsorption capacity of Fe_3O_4-RF-MIPs is
381 much higher than that of Fe_3O_4-RF-NIPs at the same initial concentration. What is
382 more, equilibrium adsorption capacity of Fe_3O_4-RF-MIPs for SLA is calculated to be
383 36.0 mg g^{-1}, which is 4.36 times more than that of Fe_3O_4-RF-NIPs (8.25 mg g^{-1})
384 because more specific adsorption sites exist on Fe_3O_4-RF-MIPs for the recognition of
385 SLA. In addition, the adsorption capacity (9.8 mg g^{-1}) and *IF* (2.52) of
386 Fe_3O_4-RF-MIPs prepared by the one pot method (Fig. S5) are lower than those
387 synthesized by the two-step template immobilization strategy, illustrating that the
388 two-step template immobilization strategy makes Fe_3O_4-RF-MIPs having more
389 ordered and evenly distributed imprinted sites attached on the surface of carriers.

Further, as shown in Fig. 6D, the adsorption equilibrium data for both Fe_3O_4-RF-MIPs and Fe_3O_4-RF-NIPs are fit to Freundlich isotherms model ($R^2 > 0.99$). Table S1 exhibits relevant isotherm parameters and equations. The results demonstrate that the adsorption occurs on specific homogeneous sites and the adsorption of SLA onto Fe_3O_4-RF-MIPs could be a multilevel adsorption process [43].

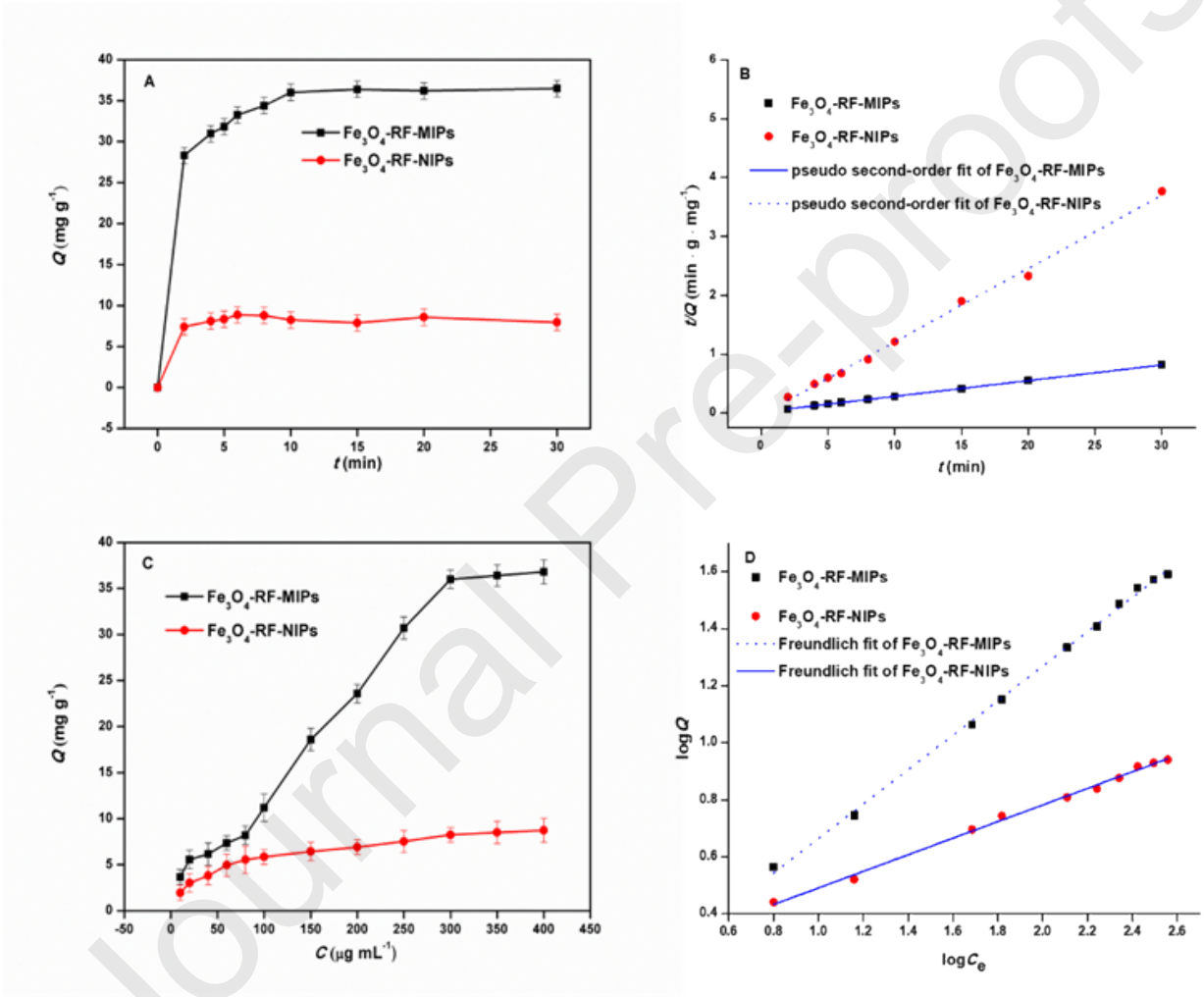

Fig. 6. Adsorption kinetic (A) and isothermal (C) curves of Fe_3O_4-RF-MIPs and Fe_3O_4-RF-NIPs for the SLA; Pseudo-second-order model (B) and Freundlich isotherms model (D) to evaluate the kinetic and isothermal mechanism of Fe_3O_4-RF-MIPs and Fe_3O_4-RF-NIPs.

3.5. Adsorption selectivity

To evaluate the adsorption selectivity of Fe_3O_4-RF-MIPs and Fe_3O_4-RF-NIPs, two structural analogs (NA and IAA) and four coexistences (ID, BZD, E2, and E1) are chosen as competitors (Fig. S6). From Fig. 7, it can be seen that the adsorption amount of SLA onto Fe_3O_4-RF-MIPs is 36.0 mg g^{-1}, much higher than other experimental adsorbates. Among these, the higher adsorption amounts for NA (26.55 mg g^{-1}) and IAA (23.67 mg g^{-1}) are contributed to a partial structure similar to that of SLA. Moreover, Fe_3O_4-RF-MIPs and Fe_3O_4-RF-NIPs both have low adsorption amounts for ID (1.130 mg g^{-1}, 1.06 mg g^{-1}), BZD (1.540 mg g^{-1}, 1.36 mg g^{-1}), E1 (0.510 mg g^{-1}, 0.46 mg g^{-1}), and E2 (0.620 mg g^{-1}, 0.55 mg g^{-1}) because of lacking of similar structures compared to NA and IAA. The specific recognition performance of the Fe_3O_4-RF-MIPs is further evaluated by *IF* and *SC* (Table 1). The *IF* value for SLA (4.36) is larger than those of the reference compounds and the *SC* values are greater than 1.26, suggesting that Fe_3O_4-RF-MIPs have high adsorption selectivity for SLA. These results all reveal outstanding specific recognition ability of Fe_3O_4-RF-MIPs.

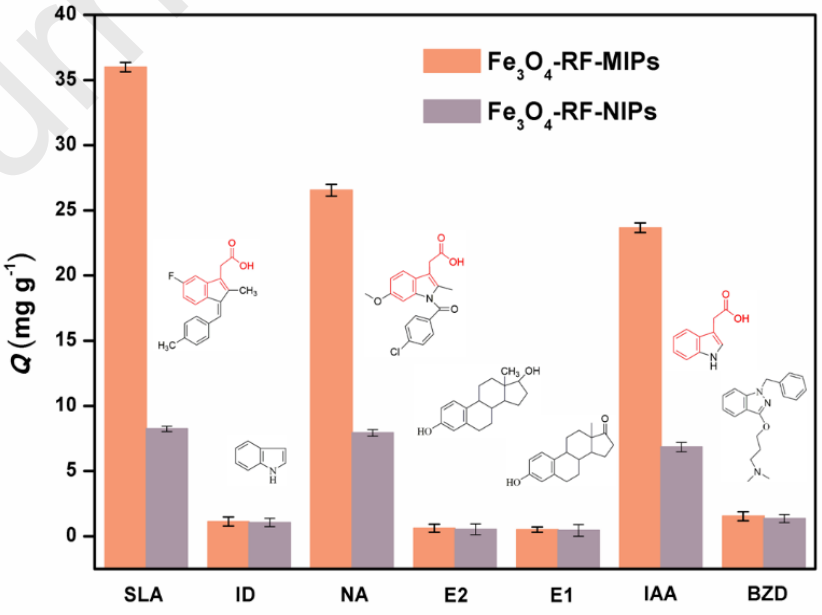

Fig. 7. Adsorption selectivity of Fe_3O_4-RF-MIPs and Fe_3O_4-RF-NIPs.

Table 1 Selectivity adsorption parameters of Fe_3O_4-RF-MIPs and Fe_3O_4-RF-NIPs.

Analytes	Q_{MIP} (mg g^{-1})	Q_{NIP} (mg g^{-1})	*IF*	*SC*
SLA	36.00	8.25	4.36	-
NA	26.55	7.94	3.34	1.31
BZD	1.540	1.36	1.13	3.86
IAA	23.67	6.85	3.45	1.26
E1	0.510	0.46	1.11	3.93
E2	0.620	0.55	1.12	3.89
ID	1.130	1.06	1.06	4.11

3.6. Reproducibility and reusability of Fe_3O_4-RF-MIPs

The reproducibility plays an important role for the utilization of materials. Based on this, the reproducibility is estimated by six different batches of Fe_3O_4-RF-MIPs prepared on different days. Five independent replicates of the adsorption for SLA are measured for each batch. The average *Q* of the six batches of Fe_3O_4-RF-MIPs is 35.89 mg g^{-1}, and the RSD are less than 6.4% (3.7%, 2.6%, 6.4%, 4.3%, 1.2%, and 5.3%) (Table S2). The results exhibit that the reproducibility of the resultant materials is satisfactory.

To investigate the service life of obtained adsorbent, the reusability of

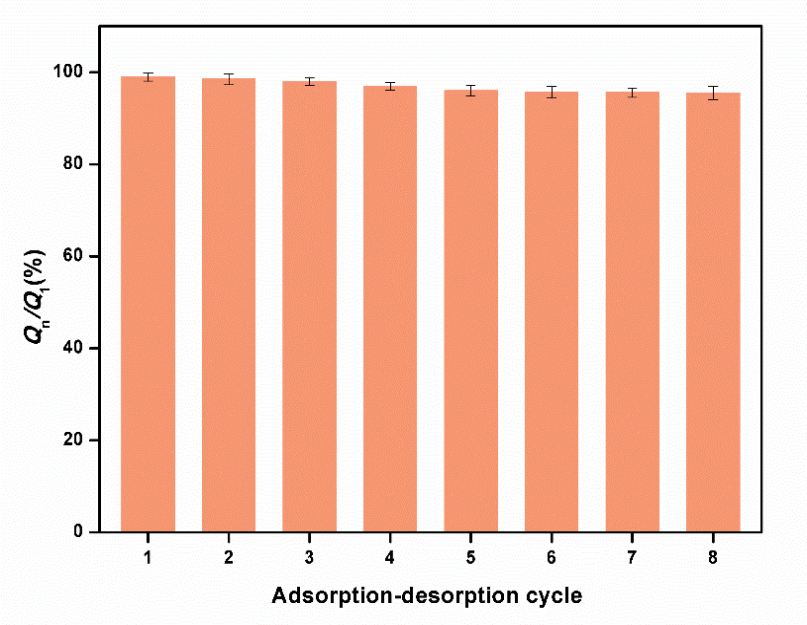

426 Fe_3O_4-RF-MIPs is tested. The eluent of ethanol-HAc (95:5, v/v) is used to desorb the
427 SLA absorbed by Fe_3O_4-RF-MIPs. Through HPLC measurement, the adsorption and
428 desorption capacities of prepared nanomaterials are depicted in Fig. 8. With the
429 increase of the cycle times, the adsorption capacity of Fe_3O_4-RF-MIPs decreases
430 slightly, but the adsorption efficiency remains above 95% after the eighth recycling,
431 which is possible concluded that the selected eluent is able to effectively destroy the
432 noncovalent interaction between SLA template molecules and imprinted sites without
433 additional damage to the shape and size of the imprinted sites. (Supporting
434 Information). The results indicate that the reusability of Fe_3O_4-RF-MIPs is
435 satisfactory with reversible recognition, interaction, and adsorption processes and the
436 eluent is suitable for reusability procedure.

437 Fig. 8. Reusability of Fe_3O_4-RF-MIPs.

438 *3.7. Method evaluation and sewage sample analysis*

439 We have established a method for the determination of SLA in sewage by using
440 Fe_3O_4-RF-MIPs as SPE materials combined with HPLC. Table 2 shows the analytical
441 performance parameters of the developed method, including linear range, LOD, LOQ,
442 and precisions. The relatively high correlation coefficient ($R^2 > 0.9971$) is obtained in
443 the range of 0.01-120 μg mL^{-1} for SLA. The LOD (S/N = 3) and LOQ (S/N = 10) are
444 as low as 2.1 ng mL^{-1} and 7.1 ng mL^{-1}, respectively. The intra-day and inter-day
445 precisions are studied through extraction and determination of SLA in the spiked
446 sewage at three different levels (0.01, 0.05, and 0.5 μg mL^{-1}). The results demonstrate
447 that the relative standard deviation (RSD) of intra-day precision is 1.6-3.8%, while

that of inter-day precision is 2.4-4.9%.

Table 2. The performance parameters of the proposed method. (n = 5)

Analyte	Linearity range (μg mL^{-1})	R^2	RSD (%)		LOD (ng mL^{-1})	LOQ (ng mL^{-1})
			intra-day	inter-day		
SLA	0.01-120	0.9971	1.6-3.8	2.4-4.9	2.1	7.1

To verify the accuracy of the established method, the sewage samples spiked with three levels (0.01, 0.05, and 0.5 μg mL^{-1}) of SLA were analyzed by HPLC and each concentration was measured five times. From Table 3, the recoveries of SLA in sewage from a hospital and a pharmaceutical plant samples are ranged from 93.2% to 97.4%, and 94.6% to 98.6%, respectively. The RSDs are less than 5.2%. These results reveal that the developed method is accurate, sensitive, and selective for determination of SLA in sewage and the Fe_3O_4-RF-MIPs coupled with HPLC can meet the need of selective isolation and determination of trace SLA in sewage. Compared with previous methods [47,48] for detecting SLA by HPLC with traditional SPE and photo-diode array detection, the established method has lower LODs and higher recoveries in two different sewage samples (Table S3).

Table 3. Recoveries of Fe_3O_4-RF-MIPs towards SLA for spiked sewage sample analysis. (n=5)

Sample	SLA					
	0.01 μg mL^{-1}		0.05 μg mL^{-1}		0.5 μg mL^{-1}	
	Recovery(%)	RSD(%)	Recovery(%)	RSD(%)	Recovery(%)	RSD(%)
hospital	93.2	5.2	95.3	4.7	97.4	3.2
pharmaceutical plant	94.6	4.9	96.6	4.2	98.6	2.8

Fig. 9 presents the chromatograms of the standard solution with SLA, the spiked sewage samples, and eluent of adsorbed Fe_3O_4-RF-MIPs. As shown in Fig. 9A-b and 9B-b, the peak of SLA could not be observed and some other peaks in spiked sewage

samples (0.05 μg mL^{-1}), suggesting that the sewage samples are complex matrices. After absorbing and enriching of sewage samples, Fe_3O_4-RF-MIPs are eluted with ethanol-HAc (95:5, v/v) and the eluents were detected (Fig. 9A-c and 9B-c). The peak of SLA emerges distinctly at about 5.4 min with no interfering peaks, which is in accordance with the retention time of standard SLA (Fig. 9A-a, 9B-a). The results prove that Fe_3O_4-RF-MIPs combining with HPLC can selectively and efficiently absorb, enrich, and detect trace SLA in the sewage.

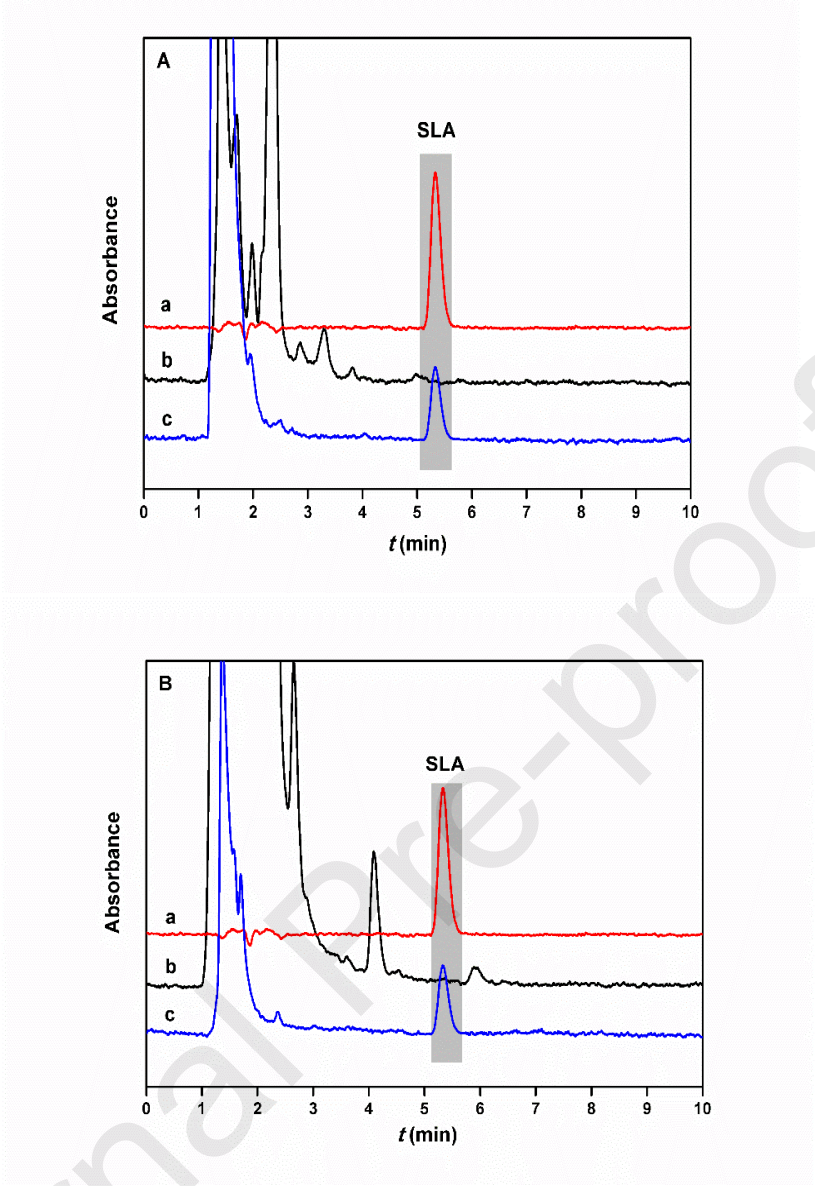

Fig. 9. Chromatograms of wastewater samples from a hospital (A) and a pharmaceutical plant (B) spiked samples with SLA at the concentration of 0.05 μg mL^{-1} (b), eluent of adsorbed Fe_3O_4-RF-MIPs (c), and SLA standard solution (a).

4. Conclusion

In summary, a novel kind of hydrophilic imprinted magnetic nanomaterials was fabricated for the specific recognition of SLA by adopting a two-step template immobilization strategy of surface molecular imprinting technique. The resorcinol and formaldehyde are first proposed as functional monomers to form hydrophilic

480 imprinted layer, which is beneficial for the imprinting performances, in virtue of its
481 rich hydrophilic functional groups and good compatibility with the water matrix. The
482 resultant nanomaterials not only exhibit outstanding magnetic performance for rapid
483 separation, but also show the high adsorption capacity (36 mg g^{-1}), satisfactory
484 selectivity (*IF* = 4.36, *SC* > 1.2) and excellent reusability. Meanwhile,
485 Fe_3O_4-RF-MIPs combined with HPLC are successfully applied in the specific
486 isolation and detection of SLA in sewage samples. It is proved that the established
487 method has good accuracy, precision, and sensitivity because of low LOD (2.1 ng
488 mL^{-1}) and LOQ (7.1 ng mL^{-1}), little RSDs (≤ 5.2%), and high recoveries (≥ 93.2%).
489 All these results indicate that Fe_3O_4-RF-MIPs, owning the strong specific binding
490 ability and outstanding dispersibility in sewage, have a promising future in selective
491 recognition and determination of SLA from environmental water.

492 ## Acknowledgments

493 This work was supported by the National Natural Science Foundation of China
494 (Nos. 21305107, 81701830), the Natural Science Foundation of Shaanxi Province
495 (Nos. 2017JM2010, 2017JQ8052), the Fundamental Research Funds for the Central
496 Universities (Nos. xjj2017028, xjj2016101), and China Postdoctoral Science
497 Foundation (Nos. 2016M600800, 2014M562388). The authors thank Junjie Zhang,
498 School of Science, Xi'an Jiaotong University, for the help with FT-IR characterization.
499 The authors are appreciate the assistance of Instrumental Analysis Center of Xi'an
500 Jiaotong University for the VSM analysis.

Appendix A. Supplementary material

Supplementary data associated with this article can be found in the online version.

References:

[1] H.M. Sun, W. Ting, Z.C. Yang, C. Yu, W.Z. Wu, Simultaneous removal of nitrogen and pharmaceutical and personal care products from the effluent of waste water treatment plants using aerated solid-phase denitrification system, Bioresour. Technol. 287 (2019) 121389.

[2] S. Suarez, J.M. Lema, F. Omil, Removal of Pharmaceutical and Personal Care Products (PPCPs) under nitrifying and denitrifying conditions, Water Res. 44 (2010) 3214-3224.

[3] A.K. Berg, S.J. Mandrekar, K.L.A. Ziegler, E.C. Carlson, E. Szabo, M.M. Ames, D. Boring, P.J. Limburg, J.M. Reid, Population pharmacokinetic model for cancer chemoprevention with sulindac in healthy subjects, J. Clin. Pharmacol. 53 (2013) 403-412.

[4] D.F. Martin, J.M. Martin, T.A. Ward, Removal of selected NSAIDs (nonsteroidal anti-inflammatory drugs) in aqueous samples by octolig, J. Environ. Sci. Health., Part A Environ. Sci. Eng. Toxic Hazard. Subst. Control 51 (2016) 186-191.

[5] T.M. Penning, Inhibition of 5 beta-dihydrocortisone reduction in rat liver cytosol: a rapid spectrophotometric screen for nonsteroidal anti-inflammatory drug potency, J. Pharm. Sci. 74 (1985) 651-654.

[6] C.H. Hsu, Y.J. Cheng, B. Singco, H.Y. Huang, Analyses of non-steroidal anti-inflammatory drugs by on-line concentration capillary electrochromatography

using poly(stearyl methacrylate-divinylbenzene) monolithic columns, J. Chromatogr. A 1218 (2011) 350-358.

[7] F. Krier, M. Brion, B. Debrus, P. Lebrun, A. Driesen, E. Ziemons, B. Evrard, P. Hubert, Optimisation and validation of a fast HPLC method for the quantification of sulindac and its related impurities, J. Pharm. Biomed. Anal. 54 (2011) 694-700.

[8] J. Lenik, Preparation and characterization of a sulindac sensor based on PVC/TOA-SUL membrane, Mater. Sci. Eng. C 37 (2014) 383-389.

[9] W.H. Huang, L. Shao, S.X. Li, D. Guo, L.S. Wang, Z. Li, X.D. Peng, Y. Chen, W. Zhang, H.H. Zhou, Z.R. Tan, Simultaneous determination of sulindac and its metabolites sulindac sulfide and sulindac sulfone in human plasma by a sensitive UPLC-PDA method for a pharmacokinetic study, Anal. Methods 6 (2014) 4679-4685.

[10] P.B. Fayad, M. Prévost, S. Sauvé, On-line solid-phase extraction coupled to liquid chromatography tandem mass spectrometry optimized for the analysis of steroid hormones in urban wastewaters, Talanta 115 (2013) 349-360.

[11] B. Wang, X. Zhao, X. Xie, K.Z. Xie, G.X. Zhang, T. Zhang, X.Z. Liu, Development of an accelerated solvent extraction approach for quantitative analysis of chloramphenicol, thiamphenicol, florfenicol, and florfenicol amine in poultry eggs, Food Anal. Methods 12 (2019) 1705-1714.

[12] S.C. Wang, P.P. Qi, S.S. Di, J. Wang, S.G. Wu, X.Y. Wang, Z.W. Wang, Q. Wang, X.Q. Wang, C.S. Zhao, Q. Li, Significant role of supercritical fluid chromatography-mass spectrometry in improving the matrix effect and analytical

efficiency during multi-pesticides residue analysis of complex chrysanthemum samples, Anal. Chim. Acta 1074 (2019) 108-116.

[13] Z.Y. Zhu, W.T. Bai, Y. Xu, H.Z. Gong, Y.L. Wang, D.M. Xu, J. Gao, Liquid-liquid extraction of methanol from its mixtures with hexane using three imidazolium-based ionic liquids, J. Chem. Thermodyn. 138 (2019) 189-195.

[14] M.M. Wang, F.Y. Ye, H. Wang, H. Admassu, M.A.A. Gasmalla, X. Hua, R.J. Yang, High efficiency selective and reversible capture of lactulose using new boronic acid-functionalized porous polymeric monoliths, Chem. Eng. J. 370 (2019) 1274-1285.

[15] D.M. Gao, Z.P. Zhang, M.H. Wu, C.G. Xie, G.J. Guan, D.P. Wang, A surface functional monomer-directing strategy for highly dense imprinting of TNT at surface of silica nanoparticles, J. Am. Chem. Soc. 129 (2007) 7859-7866.

[16] Y.R. Xu, X.L. Hu, P. Guan, C.B. Du, Y. Tian, S.C. Ding, Z.L. Li, C.R. Yan, A novel controllable molecularly imprinted drug delivery system based on the photothermal effect of graphene oxide quantum dots, J. Mater. Sci. 54 (2019) 9124-9139.

[17] M.N. Ding, D.C. Sorescu, A. Star, Photoinduced charge transfer and acetone sensitivity of single-walled carbon nanotube-titanium dioxide hybrids, J. Am. Chem. Soc. 135 (2013) 9015-9022.

[18] Z.L. Zhang, X.D. Zhang, D.C. Niu, Y.S. Li, J.L. Shi, Highly efficient and selective removal of trace lead from aqueous solutions by hollow mesoporous silica loaded with molecularly imprinted polymers, J. Hazard. Mater. 328 (2017) 160-169.

[19] M. Zhang, B.Y. Wang, Y.W. Zhang, W.Z. Li, W.J. Gan, J.L. Xu, Facile synthesis of magnetic hierarchical copper silicate hollow nanotubes for efficient adsorption and removal of hemoglobin, Dalton Trans. 45 (2016) 922-927.

[20] M. Dinc, C. Esen, B. Mizaikoff, Recent advances on core-shell magnetic molecularly imprinted polymers for biomacromolecules, Trends Anal. Chem. 114 (2019) 202-217.

[21] D.X. Fan, L. Jia, H.Y. Xiang, M.J. Peng, H. Li, S.Y. Shi, Synthesis and characterization of hollow porous molecular imprinted polymers for the selective extraction and determination of caffeic acid in fruit samples, Food Chem. 224 (2017) 32-36.

[22] M. Cantarella, S.C. Carroccio, S. Dattilo, R. Avolio, R. Castaldo, C. Puglisi, V. Privitera, Molecularly imprinted polymer for selective adsorption of diclofenac from contaminated water, Chem. Eng. J. 367 (2019) 180-188.

[23] X.Y. Xie, Q. Hu, R.F. Ke, X.Y. Zhen, Y.S. Bu, S.C. Wang, Facile preparation of photonic and magnetic dual responsive protein imprinted nanomaterial for specific recognition of bovine hemoglobin, Chem. Eng. J. 371 (2019) 130-137.

[24] W.Y. Tang, K.H. Row, Novel controllable hydrophilic thermo-responsive molecularly imprinted resin adsorbent prepared in water for selective recognition of alkaloids by thermal-assisted dispersive solid phase extraction, J. Pharm. Biomed. Anal. 160 (2018) 386-396.

[25] M. Kumar, B. Ram, R. Honda, C. Poopipattana, V.D. Canh, T. Chaminda, H. Furumai, Concurrence of antibiotic resistant bacteria (ARB), viruses,

589 pharmaceuticals and personal care products (PPCPs) in ambient waters of Guwahati,
590 India: Urban vulnerability and resilience perspective, Sci. Total Environ. 693 (2019)
591 133640.
592 [26] S.A. Zaidi, Effective imprinting of an anticancer drug, 6-thioguanine, via
593 mussel-inspired self-polymerization of dopamine over reduced graphene oxide,
594 Analyst 144 (2019) 2345-2352.
595 [27] L.H. Xu, X.G. Qiao, Y. Ma, X. Zhang, Z.X. Xu, Preparation of a hydrophilic
596 molecularly imprinted polymer and its application in aolid-phase extraction to
597 determine of trace acrylamide in foods coupled with high-performance liquid
598 chromatography, Food Anal. Methods 6 (2013) 838-844.
599 [28] G.F. Zhu, G.H. Cheng, P.Y. Wang, W.W. Li, Y.C. Wang, J. Fan, Water
600 compatible imprinted polymer prepared in water for selective solid phase extraction
601 and determination of ciprofloxacin in real samples, Talanta 200 (2019) 307-315.
602 [29] T.P. Huynh, A. Wojnarowicz, M. Sosnowska, S. Srebnik, T. Benincori, F.
603 Sannicolò, F. D'Souza, W. Kutner, Cytosine derivatized bis(2,2′-bithienyl)methane
604 molecularly imprinted polymer for selective recognition of 6-thioguanine, an
605 antitumor drug, Biosens. Bioelectron. 70 (2015) 153-160.
606 [30] Y. Liu, X. Hu, L. Bai, Y.H. Jiang, J. Liu, M.J. Meng, Z.C. Liu, L. Ni, A
607 molecularly imprinted polymer placed on the surface of graphene oxide and doped
608 with Mn(II)-doped ZnS quantum dots for selective fluorometric determination of
609 acrylamide, Microchim. Acta 185 (2018) 48.
610 [31] X.J. Zhang, X.Y. Cao, P.W. Huo, Y.S. Yan, Selective adsorption of micro

611 ciprofloxacin by molecularly imprinted functionalized polymers appended onto ZnS,
612 Environ. Technol. 33 (2012) 2019-2025.
613 [32] Y.N. Yuan, C.L. Yang, T.W. Lv, F.X. Qiao, Y. Zhou, H.Y. Yan, Green
614 synthesis of hydrophilic protein-imprinted resin with specific recognition of bovine
615 serum albumin in aqueous matrix, Anal. Chim. Acta 1033 (2018) 213-220.
616 [33] M. Monier, I. Youssef, D.A. Abdel-Latif, Synthesis of imprinted styrene-maleic
617 acid functionalized resin for enantio-selective extraction of R-amphetamine, Chem.
618 Eng. J. 356 (2019) 693-701.
619 [34] M. Monier, A.M.A. El-Sokkary, Preparation of molecularly imprinted
620 cross-linked chitosan/glutaraldehyde resin for enantioselective separation of
621 L-glutamic acid, Int. J. Biol. Macromol. 47 (2010) 207-213.
622 [35] J.K. Cao, H.Y. Yan, S.G. Shen, L.G. Bai, H.Y. Liu, F.X. Qiao, Hydrophilic
623 molecularly imprinted melamine-urea-formaldehyde monolithic resin prepared in
624 water for selective recognition of plant growth regulators, Anal. Chim. Acta 943
625 (2016) 136-145.
626 [36] S.R. Liang, H.Y. Yan, J.K. Cao, Y.H. Han, S.G. Shen, L.G. Bai, Molecularly
627 imprinted phloroglucinol-formaldehyde-melamine resin prepared in a deep eutectic
628 solvent for selective recognition of clorprenaline and bambuterol in urine, Anal.
629 Chim. Acta 951 (2017) 68-77.
630 [37] T.Y. Zhou, J. Ding, Z.Y. He, J.Y. Li, Z.H. Liang, C.Y. Li, Y. Li, Y.H. Chen, L.
631 Ding, Preparation of magnetic superhydrophilic molecularly imprinted composite
632 resin based on multi-walled carbon nanotubes to detect triazines in environmental

633 water, Chem. Eng. J. 334 (2018) 2293-2302.

634 [38] H. Li, R.Q. Long, C.Y. Tong, T. Li, Y.G. Liu, S.Y. Shi, Shell thickness
635 controlled hydrophilic magnetic molecularly imprinted resins for high-efficient
636 extraction of benzoic acids in aqueous samples, Talanta 94 (2019) 969-976.

637 [39] G.Q. Fu, H.Y. He, Z.H. Chai, H.C. Chen, J. Kong, Y. Wang, Y.Z. Jiang,
638 Enhanced lysozyme imprinting over nanoparticles functionalized with carboxyl
639 groups for noncovalent template sorption, Anal. Chem. 83 (2011) 1431-1436.

640 [40] R.X. Gao, Y. Hao, L.L. Zhang, X.H. Cui, D.C. Liu, M. Zhang, Y.H. Tang, Y.S.
641 Zheng, A facile method for protein imprinting on directly carboxyl-functionalized
642 magnetic nanoparticles using non-covalent template immobilization strategy, Chem.
643 Eng. J. 284 (2016) 139-148.

644 [41] J. Zeng, Y.X. Peng, J.M. Pan, H.P. Gao, R.R. Wu, Y.J. Yin, Y.S. Yan,
645 Convenient synthesis of micron-sized macroporous polymers with dents on their
646 surfaces and excellent adsorption performance for λ-cyhalothrin, Chem. Eng. J. 266
647 (2015) 1-11.

648 [42] Q. He, J.J. Liang, L.X. Chen, S.L. Chen, H.L. Zheng, H.X. Liu, H.J. Zhang,
649 Removal of the environmental pollutant carbamazepine using molecular imprinted
650 adsorbents: Molecular simulation, adsorption properties, and mechanisms, Water
651 Res. 168 (2020) 115164.

652 [43] I. Koç, G. Baydemir, E. Bayram, H. Yavuz, A. Denizli, Selective removal of
653 17β-estradiol with molecularly imprinted particle-embedded cryogel systems, J.
654 Hazard. Mater. 192 (2011) 1819-1826.

655 [44] X. Bai, S.C. Liu, J.X. Liu, Y. Ma, W.L. Zhang, J.M. Pan, Specific uptake
656 luteolin by boronate affinity-based single-hole hollow imprinted polymers sealed in
657 dialysis bags, Chem. Eng. J. 353 (2018) 911-919.
658 [45] J.P. Lewicki, C.A. Fox, M.A. Worsley, On the synthesis and structure of
659 resorcinol-formaldehyde polymeric networks-precursors to 3D-carbon
660 macroassemblies, Polymer 69 (2015) 45-51.
661 [46] F.X. Chen, S.L. Xie, J.H. Zhang, R. Liu, Synthesis of spherical Fe_3O_4 magnetic
662 nanoparticles by co-precipitation in choline chloride/urea deep eutectic solvent,
663 Mater. Lett. 112 (2013) 177-179.
664 [47] W.H. Huang, L. Shao, S.X. Li, D. Guo, L.S. Wang, Z. Li, X.D. Peng, Y. Chen,
665 W. Zhang, H.H. Zhou, Z.R. Tan, Simultaneous determination of sulindac and its
666 metabolites sulindac sulfide and sulindac sulfone in human plasma by a sensitive
667 UPLC-PDA method for a pharmacokinetic study, Anal. Methods 6 (2014)
668 4679-4685.
669 [48] T. Hirai, S. Matsumoto, I. Kishi, Simultaneous analysis of several non-steroidal
670 anti-inflammatory drugs in human urine by high-performance liquid chromatography
671 with normal solid-phase extraction, J. Chromatogr. B 692 (1997) 375-388.

672

673 **Declaration of interests**

674

675 ☒ The authors declare that they have no known competing financial interests or personal
676 relationships that could have appeared to influence the work reported in this paper.

☐The authors declare the following financial interests/personal relationships which may be considered as potential competing interests:

Highlights

A novel type of hydrophilic molecularly imprinted polymers was prepared.

Resorcinol-formaldehyde resin as hydrophilic imprinted layer was first proposed.

Two-step template immobilization and surface imprinting strategies were combined.

The imprinted nanomaterials have high adsorption capacity and good reusability.

Specific enrichment and detection of trace sulindac from sewage samples was achieved.